Photodiagnosis and Photodynamic Therapy 26 (2019) 430–435

Contents lists available at ScienceDirect

Photodiagnosis and Photodynamic Therapy

journal homepage: www.elsevier.com/locate/pdpdt

Deep convolutional neural networks for tongue squamous cell carcinoma classification using Raman spectroscopy

Mingxin Yu[a], Hao Yan[a], Jiabin Xia[a], Lianqing Zhu[a,*], Tao Zhang[b,**], Zhihui Zhu[b], Xiaoping Lou[a], Guangkai Sun[a], Mingli Dong[a]

[a] Key Laboratory of the Ministry of Education for Optoelectronic Measurement Technology and Instrument, Beijing Information Science and Technology University, No. 6 Hongxia Road, Chaoyang District, Beijing 100015, China
[b] Department of stomatology, Peking Union Medical College Hospital, No. 1 Shuaifuyuan Wangfujing, Dongcheng District, Beijing 100730, China

ARTICLE INFO

Keywords:
Fiber optic raman
Tongue squamous cell carcinoma
Convolutional neural networks (ConvNets)
Deep learning
Spectroscopy
Raman Spectroscopy

ABSTRACT

With deep convolutional neural networks and fiber optic Raman spectroscopy, this study presents a novel classification method that discriminates tongue squamous cell carcinoma (TSCC) from non-tumorous tissue. To achieve this purpose, 24 tissues spectral data were first collected from 12 patients who had undergone a surgical resection due to the tongue squamous cell carcinomas. Then 6 blocks with each block including 1 convolutional layer and 1 max-pooling layer are used to extract the nonlinear feature representations from Raman spectra. The derived features form a representative vector, which is fed into a fully-connected network for performing classification task. Experimental results demonstrated that the proposed method achieved high sensitivity (99.31%) and specificity (94.44%). To show the superiority for the ConvNets classifier, comparison results with the state-of-the-art methods show it had a competitive classification accuracy. Moreover, these promising results may pave the way to apply the deep ConvNets model in the fiber optic Raman instrument for intra-operative evaluation of TSCC resection margins and improve patient survival.

1. Introduction

Tongue squamous cell carcinomas (TSCC) is the most common subsite of oral cavity squamous cell carcinomas (OCSCC). An effective treatment method for TSCC is tumor resection. During operation, generally, the surgeon attempts to discriminate the tumor border through visual inspection and palpation. However, statistics show that many oral resection specimens have inadequate resection margins [1–3]. This may cause a second operation and also may decrease survival due to tumor recurrence from residual cancer remaining after surgery. Therefore, a real-time and objective evaluation of resection margins has long been a surgeon's *Holy Grail* for increasing the number of adequate resections and improving the prognosis of patients with TSCC.

Raman spectroscopy is a non-destructive and inelastic light scatting technique depending on the specific vibrational modes of molecules [4,5]. Raman spectrum contains characteristic peaks that reveal biochemical information and biomolecular structures of the illuminated tissue. The technique has been used for differentiation between tumor and non-tumorous tissues in the oral cavity [6–11], including the tongue cancer [12,13]. Results demonstrated that OCSCC and healthy tissue were able to successfully be distinguished. In almost of those cases, Raman spectral data of the tissue, i.e., *ex vivo* measurement, were collected from a laboratory research-grade Raman instrument. Although the instrument can provide the high-quality Raman spectra of the tissue, it is not suited for intra-operative use due to its large size, high cost, a fixed probe and inconvenience. Raman fiber optic probe with small size is relative feasible and can employ to allow access to organs [14,15]. Thus, it is desired for *in vivo* measurement in intra-operative use [16].

Compared with spectral data from the laboratory research-grade Raman instrument, however, fiber-optic Raman spectra can be influenced by ambient light sources in operating room, e.g. operating room lights and light from windows [16]. Additionally, the probe is held by a hand during operation, it may not be kept at the same height results in making inconsistence intensity on Raman spectrum. These issues have a great impact on the quality of Raman spectra and the accuracy of TSCC

* Corresponding author.
** Co-corresponding author.
E-mail addresses: mingxinbit@gmail.com (M. Yu), hao_yan_1@sohu.com (H. Yan), xiajiabinxjb@gmail.com (J. Xia), lianqingzhubistu@163.com (L. Zhu), drtzhang@126.com (T. Zhang), 18698105576@163.com (Z. Zhu), louxiaoping@bistu.edu.cn (X. Lou), guangkai_sun@sohu.com (G. Sun), minglibistu@sina.com (M. Dong).

https://doi.org/10.1016/j.pdpdt.2019.05.008
Received 3 April 2019; Received in revised form 30 April 2019; Accepted 9 May 2019
Available online 10 May 2019
1572-1000/ © 2019 Elsevier B.V. All rights reserved.

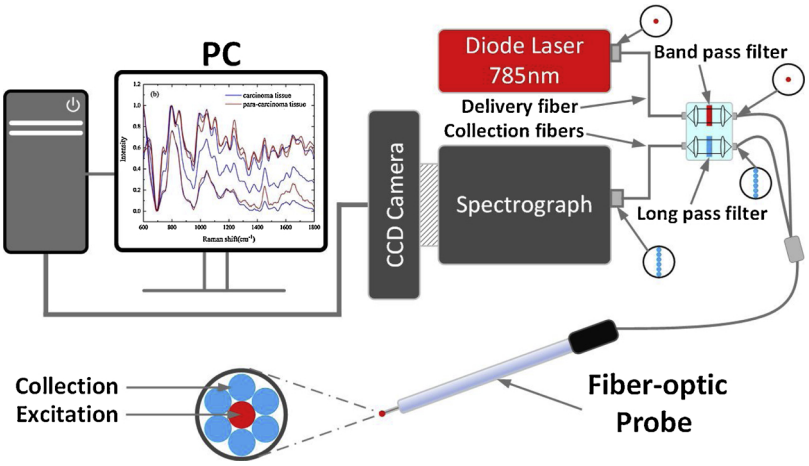

Fig. 1. Schematic description of fiber optic Raman spectroscopy system.

detection. Thus, the most important step is to develop an effective method for improving the robustness of the TSCC classification [17].

A variety of methods for OCSCC classification have been used in the context of Raman spectroscopy [18–25]. Among them, combined principle component analysis (PCA) with linear discriminate analysis (LDA) can be regarded as a popular method for automatic OCSCC classification. Firstly, PCA is used to reduce dimensionality of Raman spectra for extracting features [26]. Then, an LDA classifier is trained using the extracted features [27]. Lastly, OCSCC and other tissues, e.g. healthy tissue, can be recognized by the trained LDA classifier. Experimental results demonstrated that this method obtained high specificity, sensitivity and accuracy of OCSCC classification. To our knowledge, however, very little work provides an effective method for TSCC classification (most common subsite of OCSCC) of Raman spectra from the fiber optic probe.

To be specific, conventional methods rely too much on features extraction, which can be thought as a hand-engineered process. However, we believe handcrafted features are not able to extract enough feature representations, so complex Raman spectral data is not able to be dealt with well. Recently, deep learning as a branch of machine learning that takes advantage of multiple layers of linear and non-linear processing units to learn hierarchical representations of features from input data. It can be seen as an end-to-end learning method which identifies unseen examples without the need for feature engineering. Convolutional Neural Networks (ConvNets) as a predominant method of deep learning has been successfully used in many fields, such as image classification, audio recognition, etc., [28–36]. ConvNets can extract and learn local, low-level features from input data by using convolutions, which are key components, and then form global and high-level features in deeper layers. Motived by the recent and widespread success of ConvNets, this paper presents capacity of fiber optic Raman spectroscopy combined with the ConvNets for TSCC classification. The proposed method could take as an effective solution used for the Raman instrument with fiber optic probe, its aim is to improve the robustness of TSCC classification and could be applied in intra-operative use in the future.

2. Materials and methods

2.1. Sample collection and preparation

At the department of stomatology, Peking Union Medical College Hospital, 24 samples were collected from 12 patients who had undergone a surgical resection due to the tongue squamous cell carcinomas. Informed consent was obtained prior to the operation according to the protocol approved by the Medical Ethics Committee of Peking Union Medical College Hospital.

Twenty-four samples contained TSCC and non-tumorous tissue. Twelve samples were collected from the fresh resection specimens, which were cut from a region with macroscopically visible tumor by the surgeon during operation. The other twelve samples contained only non-tumorous tissue and were collected from the resection specimen within a macroscopically normal appearing region adjacent to the tumor. Samples from surgical resection specimens were taken within 20 min. For each patient, in order to minimize the impact on the quality of the fresh tissue, the samples were kept in cold saline (0.9% NaCl) prior to Raman spectroscopy measurements.

2.2. Acquiring raman spectra

Raman spectra were required from the surface of the tumor and non-tumorous tissues using Raman system. This system mainly consists of a spectrum stabilized 785 nm diode laser with maximum power 300 mW (FC-D-785 nm, Changchun New Industries Optoelectronics Technology Co., Ltd. China), scientific-grade spectrometer (QE65PRO-RAMAN, Ocean Optics, USA), charged-coupled device with low etalon (S7031 − 1006, Hamamatsu, Japan), and fiber-optic Raman probe (Beijing Scitlion Technology corp., LTD, China). Fig. 1 shows the block diagram of the fiber optic Raman spectroscopy system.

To be specific, the Raman probe with the size of 1.0 mm diameter contained a central light delivery fiber and 6 collection fibers. The central fiber is surrounded by the collection fibers. The size of diameter for each fiber is 100 μm and the numerical aperture (NA) is 0.22. Two stages of optical filtering are placed at the proximal and distal ends of the probe so that maximizing the collection of tissue Raman signals, while effectively suppressing the interference of Rayleigh scattered laser light, fiber fluorescence and silica Raman signals. In this system, the power of laser is set to 100 mW and the spatial resolution is 100 μm. All spectrums were recorded in the spectral range from 300 to 3950 cm^{-1}, using a spectral resolution of 6 cm^{-1}.

For the recording of Raman spectrum, each sample with at least the size of 10 × 10 mm was put on a special tissue culture dish. Considering the interference of ambient light in the operation room, we simulated this effect by changing the brightness of environmental light. Three positions in each sample were selected as Raman spectroscopy measurements. From each position 20 Raman spectra were recorded from the same axial plane. An acquisition time of 20 s was used for acquiring single Raman spectrum. Each spectrum was assigned the label tumor or non-tumorous tissue based on histopathological analysis performed by the pathologists: 720 tissues were identified as tumor, 720 tissues as normal.

2.3. Preprocessing of raman spectra

Before making spectral analysis, it is necessary to preprocess Raman spectral data due to a strong fluorescence signal and noise from different background sources. A standard pipeline for the preprocessing includes in the following order: smoothing, baseline correction, and normalization. Firstly, the spectra are smoothed by employing a Savitzky-Golay filter, which uses a polynomial kernel of order 3 and a span of 5 points at a time. To be specific, the purpose of the polynomial fit is used to estimate the fluorescence background and then subtract from original spectrum. Secondly, a “msbackadj” function is used as a method for baseline correction. Before adjustment, the baseline is regressed using the spline approximation. Lastly, to compare the changes in relative peak intensity in different samples, all spectra are vector-normalized.

2.4. Deep convolutional neural networks

The ConvNets contains three types of layers: convolution, pooling, and fully-connected. In our study, the input to the ConvNets is one dimensional Raman spectral data. Thus, we train one-dimensional kernels in our ConvNets model. The structure of the proposed deep ConvNets is shown in Fig. 2. It is made up of 6 blocks and 1 classification block. To be specific, each block has 6 convolutional layers and 6 pooling layers. The classification block contains 1 fully-connected layer and 1 output layer.

The purpose for using the convolutional layer is to obtain significant features from the Raman spectra. The convolution is performed by sliding the kernel over the input to produce feature maps using this equation:

$$c_m = \sum_{n=0}^{N-1} k_n x_{m-n} \quad (1)$$

where c, k, and x denote output, filter, and input, respectively, N is the number of input data points in x. The n indicates the n th element of the filter vector while m denotes the m th output element which is computed. From 0 to output N-1, the element k_n is multiplied by the element from the input x_{m-n}. These product are summed to produce the output. The rectified linear unit activation (ReLU) is applied after the convolution operation. It is employed as the activation function for blocks 1, 3, 5, 7, 9, 11. The ReLU is expressed as:

$$\mathrm{ReLU}(c_m) = \max(0, c_m) \quad (2)$$

The pooling layer employs a max-pooling operation. Within 2 stride window the largest value is retained after the max-pooling operation. Its purpose is to decrease the size of the feature map and preserve the significant features. The fully-connected layer with 2048 neurons is connected to output with 1 neuron. The output from the fully-connected layer is fed into a softmax function to predict the class by determining the class probability of each spectrum as being non-tumorous tissue or TSCC. The number of neurons, filter size, and stride in each layer are summarized in Table 1.

ConvNets is a data hungry model. To reduce the data volume requirements, we choose the data augmentation method for increasing five times size of the spectra datasets. Additionally, to avoid overfitting and improve generalization, the dropout technique is applied to the fully-connected layer. The probability of dropout is set to 0.5.

The training of the deep ConvNets is performed using Adam algorithm with learning rate equal to 1e-5, $\beta_1 = 0.9$, $\beta_2 = 0.999$, and $\varepsilon = 0.9$. Training was performed on a single NVIDIA TITAN V GPU and a computer with Intel Core i7-8700k (3.70 GHz).

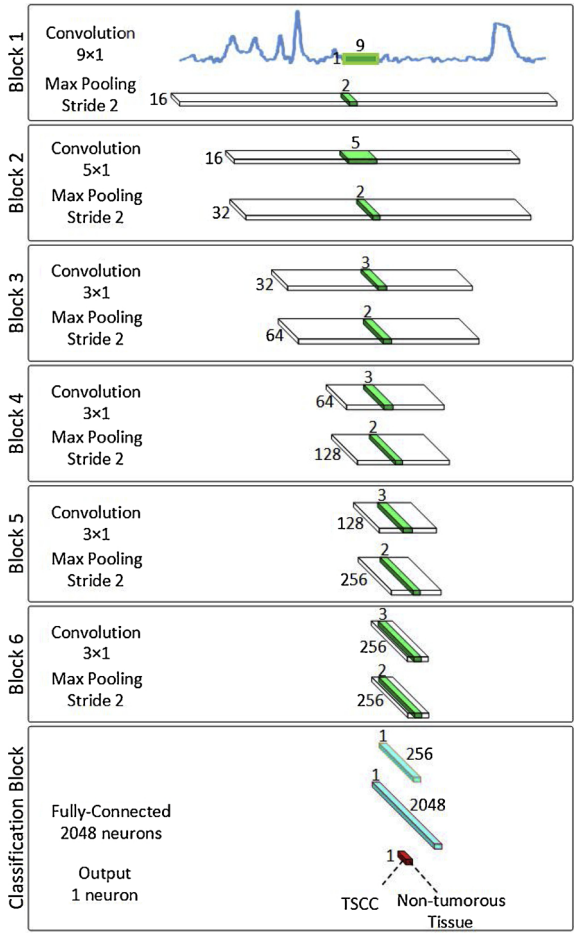

Fig. 2. The architecture of the proposed ConvNets model.

3. Results

3.1. Spectral data analysis

Mean Raman spectra of non-tumorous tissues and TSCC samples are shown in Fig. 3. For the purpose of reader clarity, normalized mean spectra of TSCC are shown in red color (dashed line), whereas, the mean spectra of non-tumorous tissues are shown in blue color (solid line). Although two types of tissues have an almost similar pattern, there is a precise difference in the intensity of Raman shifts. The obvious variations for Raman intensities are placed at 798, 846, 926, 993, 1236, 1299, 1577, 1605, 1708, and 1770 cm^{-1} [37,38]. TSCC constitutes different biomolecular components such as proteins, lipids, amino acids, carbohydrates, etc. Among them, nucleic acid and amino acid are particularly prominent [39]. The detailed information for

Table 1
Parameters of the ConvNets architecture.

layers	Type	Number of neurons	Filter Size	Stride
Block 1	Convolution	212 × 16	9	1
	Max-pooling	106 × 16	2	2
Block 2	Convolution	102 × 32	5	1
	Max-pooling	51 × 32	2	2
Block 3	Convolution	49 × 64	3	1
	Max-pooling	24 × 64	2	2
Block 4	Convolution	22 × 128	3	1
	Max-pooling	11 × 128	2	2
Block 5	Convolution	9 × 256	3	1
	Max-pooling	4 × 256	2	2
Block 6	Convolution	2 × 256	3	1
	Max-pooing	1 × 256	2	2
Classification Block	Fully-connected	2048	–	–
	Output	1	–	–

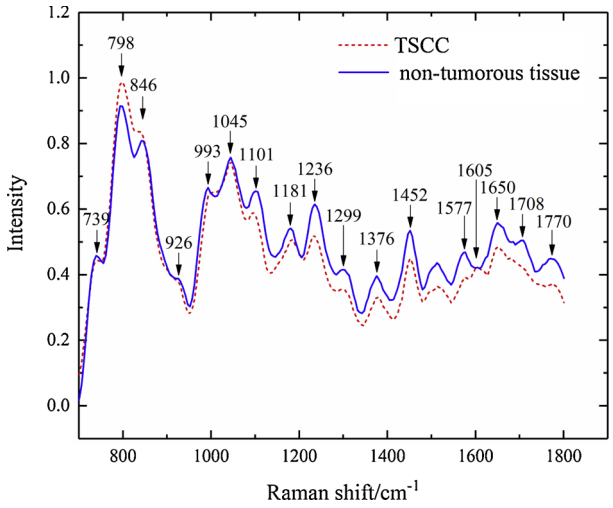

Fig. 3. The plot of the mean spectral difference between non-tumorous tissue (blue) and TSCC (red).

Table 2
Raman peaks assignment for the observed bands.

Raman shift (cm^{-1})	Peak assignment
739	Symmetric breathing of tryptophan
798	Phosphoric acid
846	Amino acids, keratin
926	C–C stretch, collagen backbone, a-helix, keratin
993	Phenylalanine
1045	Triacylglycerols
1101	Cytochrome C
1181	Typical phospholipids, phosphodiester groups in nucleic acids/collagen
1236	Amide III, keratin
1299	Fatty acid
1376	Tryptophan or phospholipid (CH3)
1452	C-H / CH2
1577	Cytochrome C, mitochondria
1605	Tyrosine, Tryptophan
1650	Amide I, C = C stretch, keratin
1708	Thymine
1770	Cholesteryl linoleate

Raman spectral peaks is listed in Table 2.

3.2. Model evaluation

To assess the generalization capability, the 5-fold cross validation method is used for evaluating the proposed deep ConvNets model. To be specific, the 80% of the dataset (4 subsets) are used as training set and remaining 20% of the dataset (1 subset) is used as the testing set. This process is repeated 5 times until all spectra are included. Its aim is to enable a different subset used as the testing data in each time. The classification performance across all five rounds of testing is averaged for the final experimental result.

The performance results obtained using confusion matrix are reported in Table 3. We observe that only one TSCC sample is misclassified as non-tumorous tissue, i.e. true positive is 143. In addition, the model wrongly provides 8 non-tumorous samples which are categorized as TSCC. General speaking, the most important metric is the true positive, since the developed model should have an ability to identify true TSCC well.

Table 3
Confusion matrix for Raman spectra.

		Predicted	
		TSCC	Non-tumorous tissue
Original	TSCC	143	1
	Non-tumorous tissue	8	136

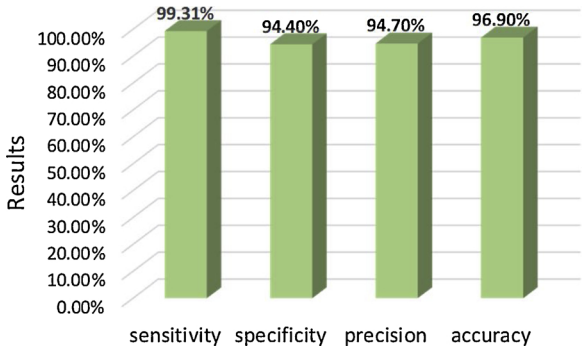

Fig. 4. The performance results of classifying non-tumorous tissue and TSCC.

Based on statistical information in confusion matrix, the average testing accuracy, precision, sensitivity, and specificity are calculated as performance evaluation metrics. The overall testing results for the proposed model are shown in Fig. 4. Specifically, the sensitivity metric has a good result which is up to 99.31%. For other three metrics, a high classification performance (> 90%) is achieved in Raman spectra.

3.3. Comparison with other methods

The proposed method has been compared with the state-of-the-art approaches. Two picking methods, i.e. PCA and SVM, PCA and LDA, were successfully used for classifying the OCSCC and non-tumorous tissue. To be specific, PCA is regarded as a feature extractor, which reduces the dimensionality of spectral data, then SVM or LDA is taken as a classifier for recognizing OCSCC from the non-tumorous tissue. Additionally, radial basis function (RBF) and polynomial kernel function are implemented in the SVM classifier. For the sake of fairness, all of approaches are performed on our dataset.

The performances (sensitivity, specificity, precision, and accuracy) obtained for each method using the Raman spectra are summarized in Table 4. It can be seen that all performance metrics achieved by our proposed deep ConvNets model outperform other methods. In particular, this model yields a sensitivity of 99.31%, which reveals that 1 of the 144 spectra annotated as the non-tumorous tissue is misclassified. The maximum misclassification of non-tumorous tissue (12/144) is occurred using the SVM with radial basis function. Analysis of the SVM with polynomial kernel function shows a specificity of 94.44%, i.e., 12 of 144 non-tumorous tissue spectra are misclassified to TSCC. For the LDA classifier, at a 97.92% of sensitivity this model produces a specificity of 88.19%. Its result was consistent with previous published results [22], which indicated higher misclassification rate on non-tumorous tissue.

Table 4
Comparison of classification results of identifying TSCC with the state-of-the-art methods.

Metrics	Our Method	SVM (RBF)	SVM(polynomial)	LDA
True positive	143	132	139	141
False positive	8	15	8	17
True negative	136	129	136	127
False negative	1	12	5	3
Sensitivity	99.31%	91.67%	96.53%	97.92%
Specificity	94.44%	89.58%	94.44%	88.19%
Precision	94.70%	89.80%	94.56%	89.24%
Accuracy	96.90%	90.62%	95.49%	93.06%

4. Discussion and conclusions

Raman fiber optic probe not only has a small size, but also can employ to allow access to organs. Therefore, fiber optic Raman spectroscopy has great potential to be used in tongue tumor resection, i.e. intra-operative use. Before developing this diagnostic tool, a solid foundation for spectroscopic knowledge is mandatory. The spectral data were collected from 12 patients with tongue squamous cell carcinomas. Analysis of Raman spectral intensities showed the obvious variations were occurred at certain wavenumbers. The biomolecular components of tongue tumor contain proteins, lipids, amino acids, carbohydrates, etc. Specially, nucleic acid and amino acid are prominent. In this study, we used those basic knowledges to develop and validate tongue squamous cell carcinomas versus non-tumorous tissue classification model.

The Raman spectral characterization of normal and tongue tumor tissue has been proved by several authors. In those researches, however, spectra were collected from a laboratory research-grade Raman instrument. For fiber-optic Raman spectra, it could be easily influenced by ambient light signal from different sources. This case would limit the detection capabilities of Raman spectroscopy since nonlinear effects overlap on the Raman spectra. Traditional methods for malignant tongue tissue classification includes PCA, SVM, and LDA. However, those methods do not encode the nonlinear effects well. Here, we demonstrated that the ConvNets was able to be used to circumvent those issues by better modeling the nonlinear interaction. The ConvNets model is capable of extracting and learning local, low-level features from input data by using convolutions, and then form global and high-level features in deeper layers. Therefore, it can model nonlinear effects and encodes information about variations in intensities at specific bands. In general, the actual intensity value at a spectral band accounts for the contribution of complex signals in the spectra.

In this study we developed fiber-optic Raman spectroscopy and deep convolutional neural networks based tissue classification model for discrimination between TSCC and non-tumorous tongue tissue. The experimental results concluded that the high sensitivity and specificity of the ConvNets model would be helpful in obtaining adequate resection margins. Overall, the proposed ConvNets method contributes an alternative way to endeavor toward developing the Raman spectroscopy instrument with the fiber optic probe for in-operative application.

Conflict of interest

The authors declare that they have no conflict of interest.

Acknowledgements

This work was supported by Program for 111 [grant number D17021], Beijing Natural Science Foundation [grant number L182066]; National Natural Science Foundation of China [grant number 51705024]. We thank all the participants who have participated in this work.

References

[1] J.K. Dillon, Cb. Brown, T.M. McDonald, D.C. Ludwig, P.J. Clark, B.G. Leroux, N.D. Futran, How does the close surgical margin impact recurrence and survival when treating oral squamous cell carcinoma? J. Oral Maxillofac. Surg. 73 (2015) 1182–1188, https://doi.org/10.1016/j.joms.2014.12.014.

[2] R.W. Smits, S. Koljenović, J.A. Hardillo, I. Ten Hove, C.A. Meeuwis, A. Sewnaik, E.A. Dronkers, T.C. Bakker Schut, T.P. Langeveld, J. Molenaar, V.N. Hegt, G.J. Puppels, R.J. Baatenburg, Resection margins in oral cancer surgery: room for improvement, Head Neck. Suppl. 1 (2015) E2197–E2203, https://doi.org/10.1002/hed.24075.

[3] D.N. Sutton, J.S. Brown, S.N. Rogers, E.D. Vaughan, J.A. Woolgar, The prognostic implications of the surgical margin in oral squamous cell carcinoma, Int. J. Oral Maxillofac. Surg. 32 (2003) 30–34, https://doi.org/10.1054/ijom.2002.0313.

[4] Y. Li, Z.N. Wen, L.J. Li, M.L. Li, N. Gao, Y.Z. Guo, Research on the Raman spectral character and diagnostic value of squamous cell carcinoma of oral mucosa, J. Raman Spectrosc. 41 (2009) 142–147, https://doi.org/10.1002/jrs.242.

[5] N. Amharref, A. Beljebbar, S. Dukic, L. Venteo, L. Schneider, M. Pluot, M. Manfai, Discriminating healthy from tumor and necrosis tissue in rat brain tissue samples by Raman spectral imaging, Biochim. Biophys. Acta 1768 (2007) 2605–2615, https://doi.org/10.1016/j.bbamem.2007.06.032.

[6] L. Su, Y.F. Sun, Y. Chen, P. Chen, A.G. Shen, X.H. Wang, J. Jia, Y.F. Zhao, X.D. Zhou, J.N. Hu, Raman spectral properties of squamous cell carcinoma of oral tissues and cells, Laser Phys. 22 (2012) 311–316, https://doi.org/10.1134/S1054660X12010185.

[7] S.P. Singh, A. Deshmukh, P. Chaturvedi, C. Murali Krishna, In vivo Raman spectroscopic identification of premalignant lesions in oral buccal mucosa, J. Biomed. Opt. 17 (2012) 105002, , https://doi.org/10.1117/1.JBO.17.10.105002.

[8] H. Krishna, S.K. Majumder, P. Chaturvedi, M. Sidramesh, P.K. Gupta, In vivo Raman spectroscopy for detection of oral neoplasia: a pilot clinical study, J. Biophotonics 7 (2014) 690–702, https://doi.org/10.1002/jbio.201300030.

[9] K. Guze, H.C. Pawluk, M. Short, H. Zeng, J. Lorch, C. Norris, S. Sonis, Pilot study: raman spectroscopy in differentiating premalignant and malignant oral lesions from normal mucosa and benign lesions in humans, Head Neck 37 (2014) 511–517, https://doi.org/10.1002/hed.23629.

[10] A. Deshmukh, S.P. Singh, P. Chaturvedi, C.M. Krishna, Raman spectroscopy of normal oral buccal mucosa tissues: study on intact and incised biopsies, J. Biomed. Opt. 16 (2011) 127004, , https://doi.org/10.1117/1.3659680.

[11] L.F. Carvalho, F. Bonnier, K. O'Callaghan, J. O'Sullivan, S. Flint, H.J. Byrne, F.M. Lyng, Raman micro-spectroscopy for rapid screening of oral squamous cell carcinoma, Exp. Mol. Pathol. 98 (2015) 502–509, https://doi.org/10.1016/j.yexmp.2015.03.027.

[12] O. Olaleye, U. Ekrikpo, O. Lyne, J. Wiseberg, Incidence and survival trends of lip, intra-oral cavity and tongue base cancers in south-east England, Ann. R. Coll. Surg. Engl. 97 (2015) 229–234, https://doi.org/10.1308/003588414X14055925061676.

[13] F.L. Cals, S. Koljenović, J.A. Hardillo, R.J. Baatenburg de Jong, T.C. Bakker Schut, G.J. Puppels, Development and validation of Raman spectroscopic classification models to discriminate tongue squamous cell carcinoma from non-timorous tissue, Oral Oncol. 60 (2016) 41–47, https://doi.org/10.1016/j.oraloncology.2016.06.012.

[14] I. Latka, S. Dochow, C. Krafft, B. Dietzek, J. Popp, Fiber optic probes for linear and nonlinear Raman applications – current trends and future development, Laser Photonics Rev. 7 (2013) 698–731, https://doi.org/10.1002/lpor.201200049.

[15] M.S. Bergholt, W. Zheng, K.Y. Ho, M. Teh, K.G. Yeoh, J.B. So, A. Shabbir, Z. Huang, Fiber-optic Raman spectroscopy probes gastric carcinogenesis in vivo at endoscopy, J. Biophotonics 6 (2013) 49–59, https://doi.org/10.1002/jbio.201200138.

[16] M. Jermyn, J. Desroches, J. Mercier, M.A. Tremblay, K. St-Arnaud, M.C. Guiot, K. Petrecca, F. Leblond, Neural networks improve brain cancer detection with Raman spectroscopy in the presence of operating room light artifacts, J. Biomed. Opt. 21 (2016) 94002, https://doi.org/10.1117/1.JBO.21.9.094002.

[17] S. Duraipandian, M. Sylvest Bergholt, W. Zheng, K. Yu Ho, M. Teh, K. Guan Yeoh, J. Bok Yan So, A. Shabbir, Z. Huang, Real-time Raman spectroscopy for in vivo, online gastric cancer diagnosis during clinical endoscopic examination, J. Biomed. Opt. 17 (2012) 081418, , https://doi.org/10.1117/1.JBO.17.8.081418.

[18] S.P. Singh, A. Deshmukh, P. Chaturvedi, C.M. Krishna, Raman spectroscopy in head and neck cancers: toward oncological applications, J. Cancer Res. Ther. Suppl. 1 (2012) S126–S132, https://doi.org/10.4103/0973-1482.92227.

[19] B. Yan, Y. Li, G. Yang, Z.N. Wen, M.L. Li, L.J. Li, Discrimination of parotid neoplasms from the normal parotid gland by use of Raman spectroscopy and support vector machine, Oral Oncol. 47 (2011) 430–435, https://doi.org/10.1016/j.oraloncology.2011.02.021.

[20] S. Devpura, J.S. Thakur, S. Sethi, V.M. Naik, R. Naik, Diagnosis of head and neck squamous cell carcinoma using Raman spectroscopy: tongue tissues, J. Raman Spectrosc. 43 (2011) 490–496, https://doi.org/10.1002/jrs.3070.

[21] A. Sahu, S. Talathi, S. Sawant, C. Murali Krishna, Classification of oral cancers using raman spectroscopy of serum, Proc. SPIE8939, Biomedical Vibrational Spectroscopy VI: Advances in Research and Industry (2014), https://doi.org/10.1117/12.2034941.

[22] L.J.C. Froukje, C. Tom, S. Bakker, S. Koljenović, G.J. Puppelsb, R.J. Baatenburg, Method development: raman spectroscopy-based histopathology of oral mucosa, J. Raman Spectrosc. 44 (2013) 963–972, https://doi.org/10.1002/jrs.4318.

[23] C. Knipfer, J. Motz, W. Adler, K. Brunner, M.T. Gebrekidan, R. Hankel, A. Agaimy, S. Will, A. Braeuer, F.W. Neukam, F. Stelzle, Raman difference spectroscopy: a non-invasive method for identification of oral squamous cell carcinoma, Biomed. Opt. Express 5 (2014) 3252–3265, https://doi.org/10.1364/BOE.5.003252.

[24] L.F.C.S. Carvalho, F. Bonnier, K. O'Callaghanb, J. O'Sullivan, S. Flint, H.J. Byrne, F. Lyng, Raman micro-spectroscopy for rapid screening of oral squamous cell carcinoma, Exp. Mol. Pathol. 98 (2015) 502–509, https://doi.org/10.1016/j.yexmp.2015.03.027.

[25] S.A. Mian, C. Yorucu, M.S. Ullah, I.U. Rehman, H.E. Colley, Raman spectroscopy can discriminate between normal, dysplastic and cancerous oral mucosa: a tissue engineering approach, J. Tissue Eng. Regen. Med. 11 (2017) 3253–3262, https://doi.org/10.1002/term.2234.

[26] I.T. Jolliffe, Principal Component Analysis, 2nd ed., Springer, New York, 2002.

[27] Tabachnick, Using Multivariate Statistics, Harper Colins College Publishers, 1996.

[28] A. Antoniades, L. Spyrou, C.C. Took, S. Sanei, Deep learning for epileptic intracranial EEG data, IEEE 26th International Workshop on Machine Learning for Signal Processing (MLSP) (2016) 1–6, https://doi.org/10.1109/MLSP.2016.7738824.

[29] M. Haijinoroozi, Z. Mao, T. Lin, Y. Huang, EEG-based prediction of driver's cognitive performance by deep convolutional neural network, Signal Process. Image Commun. 47 (2016) 549–555, https://doi.org/10.1016/j.image.2016.05.018.

[30] J. Liang, R. Lu, C. Zhang, F. Wang, Predicting seizures from electroencephalography

recordings: a knowledge transfer strategy, 2016 IEEE International Conference on Healthcare Informatics (ICHI) (2016) 184–191, https://doi.org/10.1109/ICHI.2016.27.
[31] Z. Tang, C. Li, S. Sun, Single-trail EEG classification of motor imagery using deep convolutional neural networks, Int. J. Light Electron. Optics 130 (2017) 11–18, https://doi.org/10.1016/j.ijleo.2016.10.117.
[32] Y.R. Tabar, U. Halici, A novel deep learning approach for classification of EEG motor imagery signals, J. Neural Eng. 14 (2016) 016003, , https://doi.org/10.1088/1741-2560/14/1/016003.
[33] P. Thodoroff, J. Pineau, A. Lim, learning robust features using deep learning for automatic seizure detection, 2016 Machine Learning and Healthcare Conference (MLHC 2016), (2016), pp. 178–190.
[34] S. Stober, D.J. Cameron, J.A. Grahn, Using convolutional neural networks to recognize rhythm stimuli from electroencephalography recordings, Proceedings of the 27th International Conference on Neural Information Processing Systems, (2014), pp. 1449–1457.
[35] X. Sun, C. Qian, Z. Wu, B. Luo, G. Pan, Remembered or forgotten?—an EEG-Based computational prediction approach, PLoS One 11 (2016) e0167497, , https://doi.org/10.1371/journal.pone.0167497.
[36] M.X. Yu, X.Y. Tang, Y.Z. Lin, D. Schmidt, X.Z. Wang, Y.K. Guo, B. Liang, An eye detection method based on convolutional neural networks and support vector machines, Intell. Data Anal. 22 (2018) 345–362, https://doi.org/10.3233/IDA-173361.
[37] M. Marro, C. Nieva, A. de Juan, A. Sierra, Unravelling the metabolic progression of breast Cancer cells to bone metastasis by coupling raman spectroscopy and a novel use of mcr-als algorithm, Anal. Chem. 90 (2018) 5594–5602, https://doi.org/10.1021/acs.analchem.7b04527.
[38] K. Aubertin, J. Desroches, M. Jermyn, V.Q. Trinh, F. Saad, D. Trudel, Frédéric Leblond, Combining high wavenumber and fingerprint Raman spectroscopy for the detection of prostate cancer during radical prostatectomy, Biomed. Opt. Express 9 (2018) 4294–4305, https://doi.org/10.1364/BOE.9.004294.
[39] F.L.J. Cals, S.T.C. Bakker, P.J. Caspers, D.J.R.J. Baatenburg, S. Koljenović, G.J. Puppels, Raman spectroscopic analysis of the molecular composition of oral cavity squamous cell carcinoma and healthy tongue tissue, Analyst 143 (2018) 4090–4102, https://doi.org/10.1039/c7an02106b.